Report

Current Biology

Object-Detecting Neurons in *Drosophila*

Highlights

- LC11 columnar projection neurons form an optic glomerulus in the brain
- Dendrites of individual LC11s span many individual columns and overlap each other
- LC11 is activated only by the movement of small dark visual objects
- Object selectivity and sensitivity are tuned by inhibitory currents

Authors

Mehmet F. Keleş, Mark A. Frye

Correspondence

frye@ucla.edu

In Brief

Keleş and Frye report on a novel columnar visual projection neuron in *Drosophila*. Each LC11 has a large anatomical receptive field innervating many surrounding columns of the lobula. LC11 is excited by the omni-directional movement of objects as small as 2.2° and is inhibited by larger objects or movement of the visual panorama.

Keleş & Frye, 2017, Current Biology *27*, 680–687
March 6, 2017
http://dx.doi.org/10.1016/j.cub.2017.01.012

CellPress

CellPress

Current Biology
Report

Object-Detecting Neurons in *Drosophila*

Mehmet F. Keleş[1] and Mark A. Frye[1,2,*]
[1]Department of Integrative Biology and Physiology, University of California, Los Angeles, Los Angeles, CA 90095, USA
[2]Lead Contact
*Correspondence: frye@ucla.edu
http://dx.doi.org/10.1016/j.cub.2017.01.012

SUMMARY

Many animals rely on vision to detect objects such as conspecifics, predators, and prey. Hypercomplex cells found in feline cortex and small target motion detectors found in dragonfly and hoverfly optic lobes demonstrate robust tuning for small objects, with weak or no response to larger objects or movement of the visual panorama [1–3]. However, the relationship among anatomical, molecular, and functional properties of object detection circuitry is not understood. Here we characterize a specialized object detector in *Drosophila*, the lobula columnar neuron LC11 [4]. By imaging calcium dynamics with two-photon excitation microscopy, we show that LC11 responds to the omni-directional movement of a small object darker than the background, with little or no responses to static flicker, vertically elongated bars, or panoramic gratings. LC11 dendrites innervate multiple layers of the lobula, and each dendrite spans enough columns to sample 75° of visual space, yet the area that evokes calcium responses is only 20° wide and shows robust responses to a 2.2° object spanning less than half of one facet of the compound eye. The dendrites of neighboring LC11s encode object motion retinotopically, but the axon terminals fuse into a glomerular structure in the central brain where retinotopy is lost. Blocking inhibitory ionic currents abolishes small object sensitivity and facilitates responses to elongated bars and gratings. Our results reveal high-acuity object motion detection in the *Drosophila* optic lobe.

RESULTS AND DISCUSSION

Whether flying or walking, flies readily orient toward large moving objects, such as elongated vertical bars or edges representing landscape features, and this behavior is mediated by interactions between motion vision and motion-independent feature detection [5–8]. Flies are able to perform some object-directed behaviors when directionally selective columnar motion detectors (T4 and T5) supplying the third optic ganglion (lobula plate) are silenced [6, 7, 9]. This finding supports the existence of object detection circuitry that acts independently of the canonical motion vision pathway [6]. Whereas many of the cells, circuits, and computations for motion processing by T4 and T5 and the downstream lobula plate are becoming ever clearer [10–13], the circuitry and functional role of the neighboring neuropile, the lobula, which houses 80% of all neurons in the lobula complex [14], is poorly understood in *Drosophila*.

The lobula contains more than 22 types of visual projection neurons (VPNs), including lobula columnar (LC) neurons that project to the ventrolateral protocerebrum (VLP) and form synapse-rich output domains called optic glomeruli for their structural similarity to olfactory glomeruli [4, 15, 16]. Neurons downstream of LC neurons that interconnect multiple optic glomeruli in the central brain respond to small objects [17], raising the possibility that select LCs may themselves be tuned to small objects. Optophysiological and electrophysiological methods have demonstrated that several LC neurons are broadly sensitive to visual features, such as edges or bars [18, 19], yet no study to date has thoroughly explored LC neurons with small two-dimensional objects.

We visually screened the publicly available Janelia Gal4 lines [20] and identified the R22H02-Gal4 driver that labels ~51 LC11 neurons (±4, n = 5); each LC11 neuron has dendritic arborizations in layers 2–5 of the lobula (Figures 1A–1C; Figures S1A and S1C; [16]). The dendrites of a single LC11 neuron span 14–15 lobula columns in the dorsoventral axis and six to eight columns in the anteroposterior axis (Figures 1C and 1D). Taking into account that LC11 dendrites form an ellipse in the lobula (Figure 1E), we estimated the total span of a single LC11 neuron to be 65–85 neighboring columns, thereby comprising a multipixel neuron. Considering the dendritic span (~15 × 8 columns), the number of LC11 cells (~50), and the full array of retinal ommatidia and neuropile columns (~28 × 28), it would seem that LC11 dendrites must overlap with one another rather extensively. Multicolor stochastic labeling of individual cells confirmed that LC11s overlap rather than tile the lobula (Figures 1F–1I). Sampling the inputs of many columns could underlie spatial pooling important for increased photon capture in dim light [21].

Previous work suggested that all LC11 output synapses are confined to the cognate glomerulus within the posterior VLP (PVLP) [4, 15]. We observe presynaptic sites not only in the PVLP glomerulus but also within layer 5 innervations of LC11 (Figures S1A and S1B), consistent with other findings [16]. A second distinct cell labeled by our Gal4 line is intrinsic to the lobula near the base of LC11 dendrites (Figure S1C; Supplemental Experimental Procedures). Calcium imaging from dendrites could have been contaminated by the intrinsic cell, but this seems unlikely since dendritic responses were consistently identical to cell body and axon terminal responses in LC11 (see below).

By contrast to the retinotopic organization of the columnar dendrites in the lobula, labeling a single LC11 neuron reveals

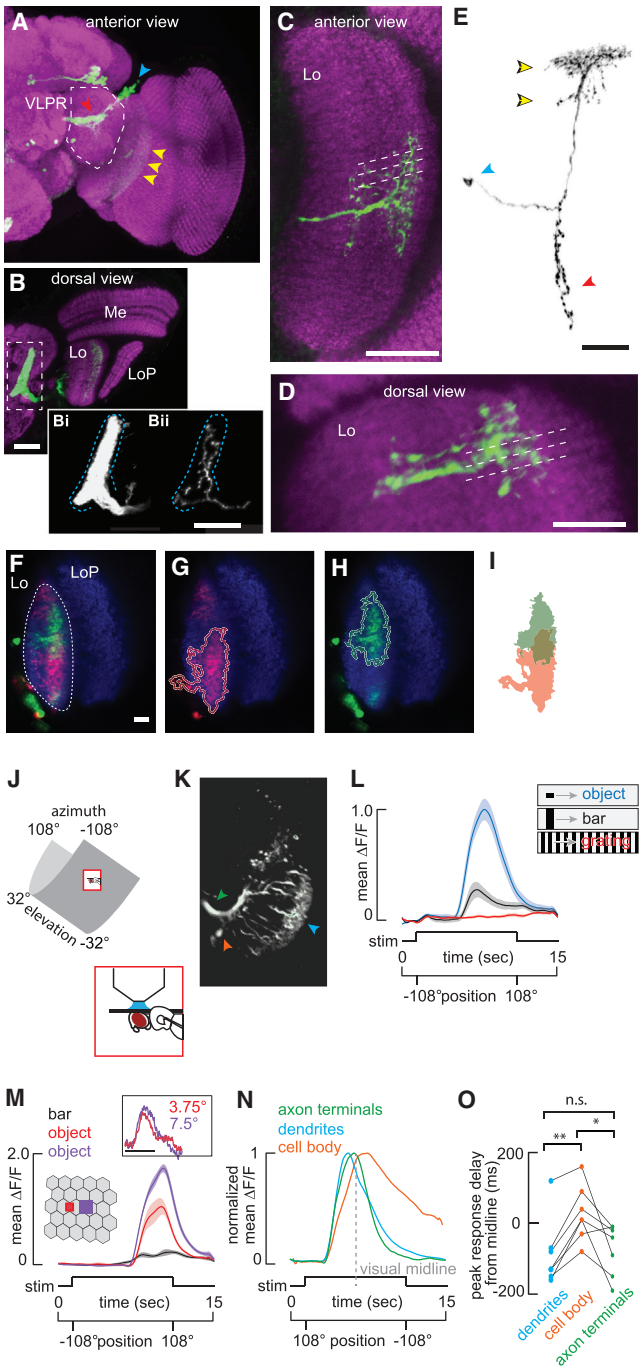

Figure 1. Anatomy and Object Selectivity of Lobula Columnar 11

(A) Maximum intensity projection of the anterior view of a brain from a fly expressing membrane-tethered GFP under the control of R22H02-Gal4 and labeled with anti-GFP (green) and nc82 (magenta). Dashed lines indicate the boundary of the ventrolateral protocerebrum. Arrowheads indicate cellular compartments; blue, cell bodies; red, terminals; yellow, dendrites.

(B) Dorsally mounted view of R22H02-Gal4>UAS-mCD8::GFP flies. Dashed rectangle indicates the unique foot-shaped LC11 glomerulus. Comparison of the labeling of ~50 LC11s innervating the glomerulus (Bi) versus stochastic labeling of a single LC11 (Bii) is shown. Single LC11 shows the full glomerular innervation with no evidence of retinotopic organization. Blue dashed line indicates the glomerular boundary. Me, medulla; Lo, lobula; LoP, lobula plate.

spatially distributed presynaptic terminals ramifying throughout the output glomerulus formed by LC11 terminals (Figures 1Bi and 1Bii). Furthermore, multicolor labeling of two individual LC11 cells (Figure S1D) shows fully interspersed axon terminals (Figures S1E and S1F). This convergent organization indicates the loss of retinotopic structure by LC11 within the glomerulus, consistent with findings in other LCs [15, 16].

To physiologically characterize LC11, we utilized GCaMP6m under two-photon imaging (Figures 1J and 1K) to record LC11 dendrites, axon terminals, and cell bodies (see Figures S1G–S1I for region of interest [ROI] images) in response to an object that may represent another fly nearby or a larger animal moving at a distance, a vertical bar that may represent a landscape feature such as a plant stalk, and a rotating wide-field grating representing optic flow generated during self-motion. We recorded from the axon terminals of LC11 (Figure S1I) and observed large responses to a 30° by 8° object (Figure 1L). The response diminished markedly for the vertical bar, and there was no response to the wide-field grating (Figure 1L). We tested whether LC11 is necessary for avoidance of similarly sized objects in flight [22], but we did not observe a clear phenotype (Figures S1J–S1L). LC11 could instead contribute to social behaviors such as courtship [9, 23]. Alternatively, given the complex spatial interactions of LC11 (see below) and its normal mode of action by individual members of the columnar array, activating or inactivating the entire population may produce spurious effects within the visual system.

Drosophila can detect and respond to objects that appear smaller than 5° [24]. We found that a moving 2.2° object drove

(C) Anterior view of a stochastic labeling of a single LC11. Dashed lines indicate individual columns within the lobula. The dendritic arbor of a single LC11 covers about 14–15 lobula retinotopic columns in this plane.

(D) Dorsal view of a single LC11. Dendritic arbors span six to seven columns in this plane.

(E) Morphology of a single LC11. Yellow arrows indicate the bistratified dendritic morphology of LC11 within lobula. Blue and red arrowheads indicate cell body and terminals, respectively. All scale bars, 25 μm.

(F–I) Single confocal plane images of multicolor stochastic labeling of LC11s. (F) Multiple cells were labeled and tagged with myristoylated smGFP attached to either HA (green) or FLAG (red) epitopes. Neuropile is labeled with nc82 (blue). The lobula is traced with a white dashed line. Scale bar, 10 μm. (G and H) Red and green channels from (F) are displayed separately with dendritic span of individual cells traced in red (G) and green (H). (I) Traced regions from (G) and (H) are shaded to show dendritic overlap. See also Figure S1.

(J–O) Two-photon imaging. (J) The fly's head is fixed and the surrounding LED arena covers 216° in azimuth and 63.2° in elevation. (K) Image of LC11s expressing GCaMP6m under two-photon microscopy. Arrowheads indicate dendrites (cyan), axon terminals forming optic glomerulus (green), and cell bodies (orange). (L) Mean GCaMP6m (±SEM shading) signal from LC11 glomerulus in response to the movement of a 30° by 8.8° object (blue), a 30° by 70° bar (black), and a wide-field grating (red, n = 7 flies). (M) Mean GCaMP6m (±SEM shading) signal from LC11 glomerulus in response to the movement of a 30° by 70° bar (black), a 2.2° square object (red), and a 4.4° square object (purple) (n = 6 flies). Inset: from tethered flies, normalized mean steering responses are shown to single-pixel impulsive displacement of objects, sizes indicated (scale bar, t = 0–100 ms; n = 10 flies). (N) Normalized mean ΔF/F of cell body (orange), dendrite (blue), and axon terminal (green) responses to the movement of a 30° by 8.8° object as in (C). Visual midline is indicated with a dashed gray line. n = 7 flies. (O) Comparison of the peak onset delay among the dendrites (blue), axon terminals (green), and cell body (orange) (*$p < 0.05$ and **$p < 0.01$, paired t test; n = 7 flies). All visual stimuli moved at 22°/s.

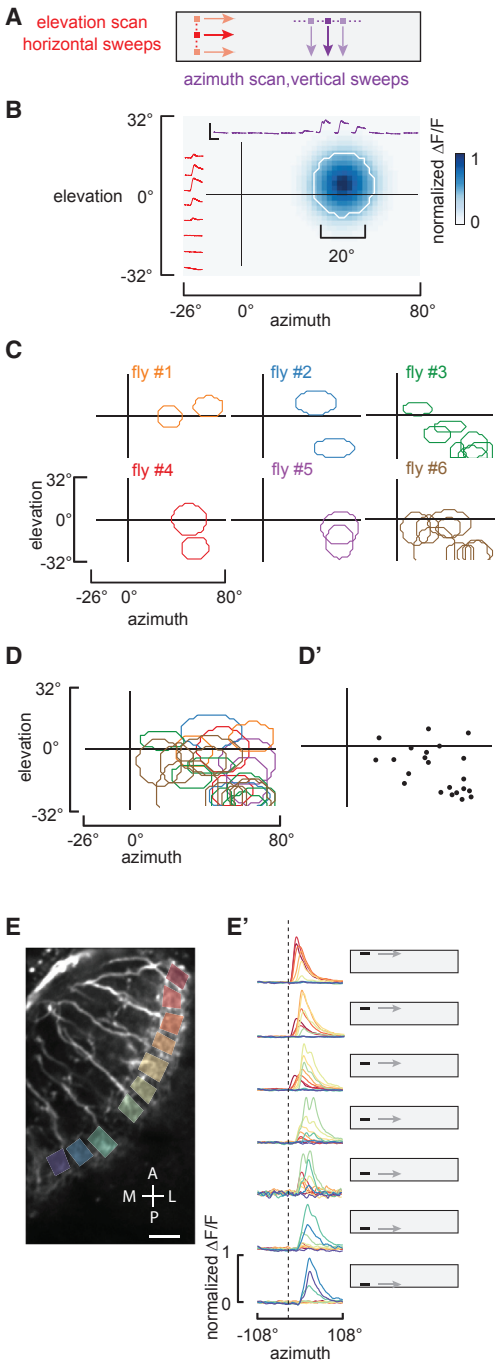

Figure 2. Individual LC11 Receptive Fields

(A) Schematic of the experimental stimuli used to map individual LC11 receptive fields from individual cell body recordings. An 8.8° square dark object was scanned along non-overlapping trajectories along both horizontal and vertical paths at 33°/s.

(B) Reconstructed receptive field of a single LC11. Individual imaging responses from a single LC11 to the horizontal and vertical sweeps are indicated in red and purple, respectively (scale bar inset represents 200% ΔF/F, 5 s). Reconstructed estimate of a single LC11 receptive field is shown in blue (see the Supplemental Experimental Procedures), and the full width at 25% maximum contour was drawn in white.

(C) Representative receptive field contours (25% maximum) from six preparations are mapped onto the projection of the visual display.

(D) The 11 receptive fields from six flies are overlaid and color coded as in (C).

(D') A dot is plotted at the centroid of each receptive field to indicate the spatial distribution of sampled LC11 recordings.

(E) To analyze the retinotopy in the dendrites of neighboring LC11 columnar cells, ROIs from separate dendritic compartments are indicated by colored boxes. An object sweep was horizontally at the elevations indicated by the cartoon display. ΔF/F responses from all ten ROIs are overlaid for each elevation. (E') To facilitate spatial comparisons, the responses are normalized to the maximum ΔF/F calcium signal at each ROI. Note that anterior (red) ROIs are activated by object motion across the top of the display, whereas posterior (blue) ROIs are activated by object motion across the bottom of the display. The dashed line indicates the earliest responses of anterior ROIs. Scale bar for the two-photon image represents 10 μm. Abbreviations for anatomical directions are as follows: A, anterior; P, posterior; M, medial; and L, lateral. See also Figure S2.

LC11 responses well above noise and greater than half-amplitude response to a 4.4° object (Figure 1M). Both objects span less than one inter-ommatidial separation angle of 5° [25]. To confirm that flies are capable of perceiving such small objects on our light-emitting diode (LED) display, we used a systems identification method during tethered flight [26] to show robust steering responses to either a single-pixel object or a two-pixel object displaced in single-pixel increments (Figure 1M, inset). In principle, any photoreceptor could respond to the luminance decrement generated by an object spanning less than its total acceptance angle, yet it is remarkable that simple hyperacuity has been documented within lobula neurons of hoverflies [3] and, more recently, within *Drosophila* photoreceptors [27].

We next compared the calcium response dynamics within dendrites, cell bodies, and axon terminals in the same preparation. Normalized response trajectories demonstrated that dendrite and terminal responses were temporally synchronized (Figure 1N), but by comparison cell bodies exhibited a significantly delayed response onset (Figure 1O) followed by a slow decay to baseline. These differences may be attributed to the unipolar morphology of some invertebrate neurons, such as LC11, in which the cell body is situated at the end of a long neurite and does not participate in synaptic integration.

Despite the slow response kinetics, imaging from the cell bodies is required to access individual neurons within the palisade of labeled LC11 cells due to the spatial intermingling of their dendrites and axon terminals (Figures S1D–S1F). To map the receptive field of individual LC11s, we swept an 8.8° square object in horizontal and vertical directions at each elevation and azimuthal angle, respectively (Figure 2A). For each LC11 recording, peak ΔF/F values were fit to Gaussian functions of azimuth and elevation and used to estimate the two-dimensional spatial receptive field (Figure 2B; Figure S2). We enclosed the spatial receptive field with a contour representing the full width at 25% maximum of the Gaussian fits (Figure 2B; see the Supplemental Experimental Procedures). We were generally able to record several distinct LC11 cell bodies from each preparation (Figure 2C). Some receptive fields that we sampled overlapped, providing functional evidence that individual LC11s have overlapping dendrites (Figure 2C). Although we did not record from all LC11s, the receptive fields of those we sampled were distributed throughout the frontolateral visual field (Figures 2D and 2D'). The average receptive field size was 24.1° by 18.8° with an SD of 5.7° and 5.7°, respectively, measured from 27 individual

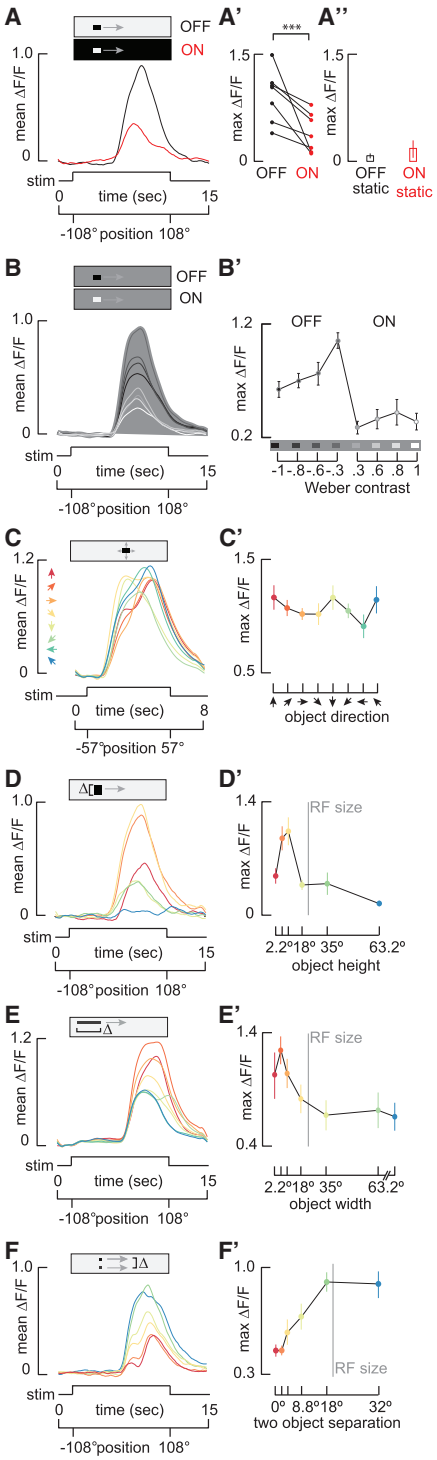

Figure 3. LC11 Is Contrast Selective, Omni-directional, and End-Stopped on the Spatial Scale of One Receptive Field

(A) Mean GCaMP6m signal from the LC11 terminal output glomerulus in response to a 30°by 8.8° moving ON object (red) and moving OFF object (black, n = 7 flies). (A'). Pairwise comparison of maximum ΔF/F of responses from each preparation (***$p < 0.001$, paired t test; n = 7 flies). (A'') Average maximum responses (±SEM) of LC11 glomerulus to a stationary 30°by 8.8°OFF and ON object placed within the hotspot of the receptive field (n = 6 flies).

cell recordings. The functional receptive field size is well below the anatomical dendritic field size (70°–75° by 30°–40°; Figure 1), a property unique to LC11 by comparison to neurons of the lamina, medulla, or lobula plate identified to date [28–30].

To confirm whether the population of LC11 dendrites samples the full visual field in a retinotopic manner, we imaged from dendritic arborizations of many LC11s simultaneously and scanned an object horizontally at varying elevation angles (Figure 2E). Objects that were presented at higher elevations elicited responses from anteriorly located dendrites (Figure 2E'). Shifting the object from higher to lower elevations on the display corresponded to shifts in calcium responses from anterior to posterior dendrites (Figure 2E'), confirming the retinotopic organization of LC11 dendritic inputs and suggesting that the visual field is sampled uniformly.

Given the sluggish on and off response kinetics observed in the cell bodies (Figure 1N), the tight temporal coupling between GCaMP responses in the dendrites and axon terminals (Figure 1N), and the innervation by individual LC11 cells throughout the output glomerulus (Figures 1Bi and 1Bii; Figures S1E and S1F), we characterized the object response properties of LC11 with recordings from the axon terminals in the VLPR. Small target motion detectors (STMDs) examined to date in the dragonfly [31] and hoverfly [3] show preference for objects darker than the background. We therefore presented a light object moving across a dark background (ON) and a dark object moving on a light background (OFF) (Figure 3A). Our results indicate that LC11 responds to both OFF and ON stimuli to varying extent, showing significant preference for OFF (Figure 3A'; paired t test, $p < 0.001$). Another characteristic feature of STMDs is flicker insensitivity [32]. Stimulating luminance increments (ON)

(B) Mean GCaMP6m signal from the LC11 glomerulus in response to varying contrast objects. Grayscale of the filled area is used to indicate the intensity of the visual background, whereas grayscale of the response line indicates the intensity of the stimulus object (n = 9 flies). The most contrasting objects do not elicit the maximum responses from LC11. (B') Average of maximum responses (±SEM) of the LC11 glomerulus to objects of varying contrast. Schematic on the x axis shows the intensity of the background compared to each object. Weber contrast values are indicated numerically (see the Supplemental Experimental Procedures; one-way ANOVA; n = 9 flies).

(C–F) LC11 glomerulus responses to (C and C') parameterized direction, (D and D') vertical height, (E and E') horizontal width, and (F and F') two-object separation distance. Time series responses are shown in (A)–(F), and color coded parameter values and maximum responses (±SEM) are shown in (C')–(F'). (C and C') LC11 is omni-directional. An 8.8° square object was moved in eight different directions in 45° steps, as indicated by the color-coded arrowheads (n = 7 flies; see single-cell responses in Figure S3). (D and D') LC11 is vertically size tuned. A 30°-wide object was moved on the same horizontal trajectory, with varied vertical heights as follows: 2.2°, 4.4°, 8.8°, 18°, 35°, and 73.2°, with colors mapped to object size in (B') (n = 7 flies). The vertical gray line indicates average receptive field (RF) size (Figure 2). (E and E') LC11 is horizontally size tuned. An object of fixed height (8.8°) and varied width (2.2°, 4.4°, 8.8°, 18°, 35°, 70°, and 210°,) was moved horizontally (n = 15 flies). The leading edge of each object appeared on the LED display at the same time. The vertical gray line indicates average estimated functional RF size (Figure 2). (F and F') LC11 is inhibited by a second object. Two 8.8° square objects moved on parallel trajectories. The distance between them was 0°, 2.2°, 4.4°, 8.8°, 18°, and 32°, with colors mapped to separation distance in C' (n = 6 flies). The vertical gray line indicates average RF size (Figure 2).

See also Figure S3.

or decrements (OFF) by a stationary object localized within the receptive failed to elicit responses in LC11 terminals (Figure 3A'').

We next systematically varied the brightness of an object moving across a fixed intensity background (Figure 3B). Interestingly, reduction of the OFF object contrast from 100% to 30% nearly doubled the amplitude of the calcium response (Figure 3B'). The object size in these experiments (30°) was chosen based on prior behavioral findings [22], yet it was larger than the estimated receptive field size (24°). It is likely that a 30° object traverses both the excitatory receptive field and the inhibitory end zones. Reducing the contrast of a sufficiently large object may in turn reduce the inhibition generated by the object edges, resulting in increased response amplitude observed in LC11 for reduced contrast (Figure 3B'). LC11 responds only weakly to moving ON objects and does not show a significant change in amplitude across contrast (Figure 3B'), providing more evidence that LC11 is OFF object specific. In flies, ON and OFF signals are separated within the lamina and relayed to deeper neuropils via parallel pathways [10, 12, 13, 33, 34]. Layers 2–4 of lobula are innervated by ON-selective Tm3 and OFF-selective Tm4 neurons [16, 35]. LC11 could potentially receive direct input from parallel ON and OFF channels via Tm3 and Tm4. Correlating a delayed OFF signal with an un-delayed ON signal arising from a single photoreceptor, i.e., within the same column, fully captured the contrast selectivity of the dragonfly STMD [31] and suggests a potential mechanism for small object sensitivity by LC11.

We next tested for directional selectivity by moving an 8.8° by 8.8° object in eight different directions. The recordings show that LC11 is not significantly selective for motion direction (Figures 3C and 3C'; one-way ANOVA, not significant [n.s.]), although it shows a slight trend for vertical directions, which is consistent with previous membrane patch-clamp recordings from the LC11 soma [19]. The glomerular output from the population of LC11s therefore serves to detect an object moving in any direction through the receptive field, a finding that we corroborated at the level of individual LC11s (Figures S3B and S3B').

The selectivity for small moving objects over elongated bars suggests that LC11 is size tuned. The classical mechanism for size tuning is end-stopped inhibition, a hypercomplex property in which an elongated contour stimulates the inhibitory end zones of a receptive field with an excitatory center [1]. We parameterized the vertical dimension of a horizontally moving object of fixed width. Note that most of our experiments move an object in the horizontal (azimuthal) direction, and thus the characteristic object size is defined as the angle subtended by the vertical edge, perpendicular to the axis of movement. The optimum LC11 response occurs for a vertical extent of 8.8°, which was one-quarter the vertical projection of the anatomical receptive field or one-half the functional receptive field (Figure 3D). The response magnitude asymptotes as the vertical size spans one functional receptive field (Figure 3D').

To test whether LC11 is size tuned in the dimension parallel with the axis of motion, we presented objects of fixed vertical height and varying horizontal widths moving horizontally. For objects of increasing width, the response amplitude peaked near 4.4° (Figure 3E). The peak amplitude decreased until the width of the object was approximately one LC11 receptive field (24°) (Figure 3E'). Note that the vertically oriented object moving horizontally generates more inhibition (Figure 3D; responses are clipped for the largest vertical bar) than an object oriented horizontally moving parallel to its orientation (Figure 3E, half-maximum response remain for the largest horizontal bar). This would be expected because the former object stimulates more ommatidia, thus activates more LC receptive fields and their presynaptic inputs, and thereby generates more spatial inhibition. Furthermore, parameterizing the vertical size of the horizontally moving object (Figure 3D), we would expect each object to sweep through different numbers of LC11 receptive fields in time, resulting in varying onset timing of the GCaMP signals in the glomerulus for each size (Figure 3D). By contrast, for the horizontally moving object, the spatial extent of the stimulus orthogonal to the motion vector is invariant, and, therefore, the leading edge stimulates the same ensemble of LC11 receptive fields for each stimulus size. Hence, the onset delay is invariant for this experiment (Figure 3E).

Owing to the close match between the spatial extent of the receptive field and optimum object size, we reasoned that the end-stopped property of LC11 could be shaped by lateral inhibition generated by nearest neighbor LC11s. If so, then the end-stopped inhibition generated by two nearby objects should be fully relieved once the objects are separated by one receptive field increment. By presenting two 8.8° square objects moving horizontally, we confirmed that, as spatial inhibition was released by increased object separation, response amplitude increased (Figure 3F). The separation distance had no effect on response amplitude once the two objects were separated by 18°, roughly the size of a single LC11's functional receptive field (Figure 3F'). Furthermore, separation distances flanking the preferred object size (8.8°) led to the biggest change in response amplitude. These results support the hypothesis that end-stopped inhibition occurs on the spatial scale of nearest neighbor LC11 functional receptive fields.

One consistent characteristic of the response to two objects is a ''double peak'' for object separation less than 18° (Figure 3E). We did not observe this bi-phasic response when presenting the same stimuli in the reverse back-to-front direction (Figures S3A and S3A'). Thus, we attribute the double peak phenomenon either to subtle differences in the spatial distribution of LC11 receptive fields converging in the axon terminals or to differences in the spatial properties of inhibition between the lateral-ventral field of view by comparison to the frontal-dorsal field.

Taken together, the results presented thus far implicate end-stop lateral inhibition in sculpting object response properties, suggesting that LC11 may receive GABAergic input. Previous immunohistochemical studies of the lobula indicate that antibodies targeting GABAergic-signaling pathways, such as glutamic acid decarboxylase (GAD), the $GABA_A$ receptor subunit RDL, and GABA itself, are present in a layer-specific manner [36, 37]. In particular, an enrichment of GABAergic neurotransmission, indicated by dense labeling of all three antibodies, is observed in layers 2 and 3 of the lobula. Our own co-labeling experiments indicate a strong overlap between the dendritic arborizations of LC11 and enriched vesicular GABA transporter (VGAT) staining (Figures 4A and 4C). In contrast, the dendrites of LC11 are spatially excluded from layer 1, known to be enriched with cholinergic signaling within T5 cells (Figures 4B and 4D) [38].

To test for functional consequences of GABAergic inhibition on the response properties of LC11, we imaged from the

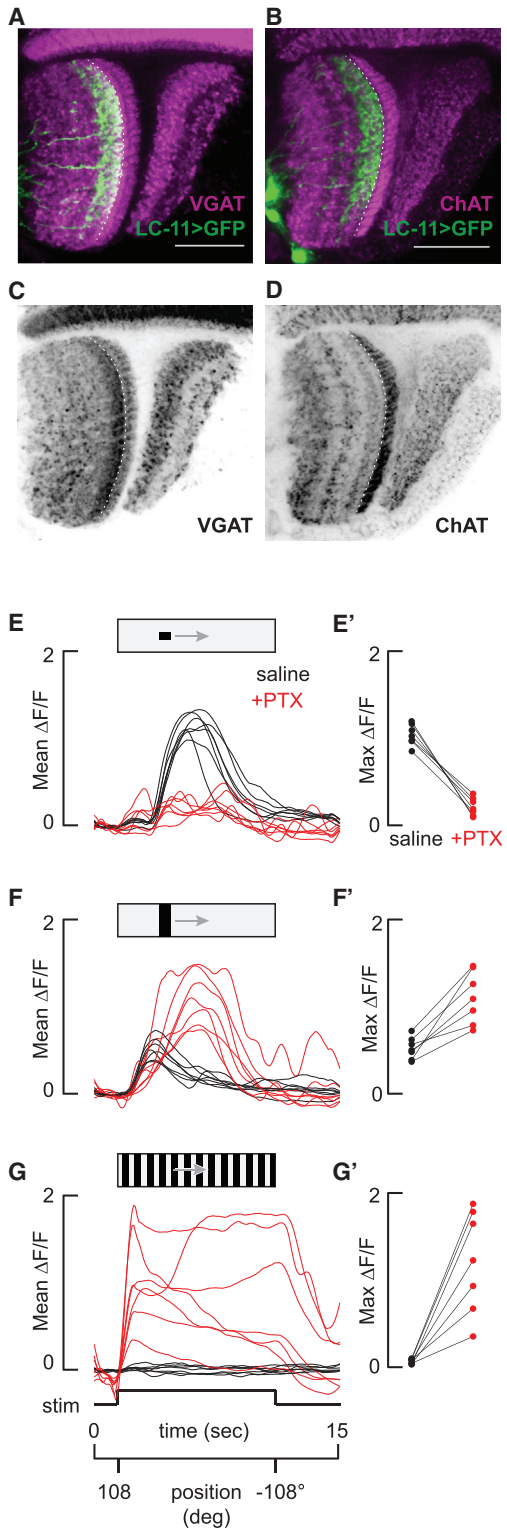

Figure 4. Both Sensitivity and Selectivity for Objects by LC11 Require Inhibition

(A and B) LC11 dendritic layer is enriched with the vesicular GABA transporter (VGAT), and the adjacent presumably presynaptic layer is enriched with choline acetyltransferase (ChAT). Dorsal view shows GFP-labeled LC11 neurons (green) co-labeled with either (A, magenta) anti-ChAT or (B, magenta) VGAT. The dashed line indicates the border between the first and second lobula strata. Scale bars, 25 μm.

(C and D) Layering of (C) VGAT and (D) ChAT is highlighted with the same labeling as in (A) and (B) but without LC11 overlaid. Scale bars, 25 μm.

(E–G) Inhibition sculpts object responses and inhibits bar and grating responses. Time series glomerular LC11 responses are shown from n = 7 flies in response to (E) a 30°by 8.8° object, (F) a 30° by 70° bar, and (G) a wide-field grating with (red) or without (black) 10 μm picrotoxin.

(E'–G') Average maximum responses from each fly (E–G) with (red) or without (black) picrotoxin.

LC11 glomerular outputs before and after blocking $GABA_A$-mediated inhibitory currents with picrotoxin (PTX). Prior to PTX application, LC11 responded robustly to an object, showed a slight excitation in response to a bar, and was not at all excited by a wide-field grating (Figures 4E–4G). Applying PTX in the perfusion saline within the same recording preparations resulted in strongly reduced object responses, large-amplitude bar responses, and large-amplitude sustained responses to wide-field motion (Figures 4E–4G). Remarkably, PTX not only resulted in a loss of selectivity for an object but also lost sensitivity to the small object itself (Figures 4E', F', and 4G'). Thus, inhibitory currents not only "end-stop" LC11 to tune its size selectivity, similar currents also actively mediate the detection of small objects. By contrast, figure-detecting cells (FDs) of the lobula plate in larger flies are excited by small-field gratings and receive GABAergic inhibition from wide-field cells, yet under GABA blockade, FDs continue to respond to small-field motion [39]. In STMDs, small object tuning has been attributed to lateral inhibition at the level of pre-synaptic neighboring ON-OFF channels that are correlated and summed [31, 40]. However, in the absence of inhibition, the model described in [31, 40] predicts that STMDs would be driven by dark edges of any size. Our finding that small object detection itself requires intact inhibition (Figure 4E) may come to promote a revised model.

The finding that LC11 dendrites span 14–15 columns of the optic lobe yet the functional receptive field is the equivalent of four to six columns wide, with peak size tuning less than the equivalent of two columns, suggests complex inhibitory spatial interactions. We propose that an excitatory-center inhibitory-surround mechanism, driven by inhibition on the spatial scale of a neighboring LC11, spatially sharpens the receptive field of LC11, making it both sensitive and selective for small contrasting objects. In summary, we show the first comprehensive physiological characterization of object selectivity by a visual projection neuron in *Drosophila*, one that shares functional properties of object detectors in other insects and vertebrates.

SUPPLEMENTAL INFORMATION

Supplemental Information includes Supplemental Experimental Procedures and three figures and can be found with this article online at http://dx.doi.org/10.1016/j.cub.2017.01.012.

AUTHOR CONTRIBUTIONS

M.F.K. and M.A.F. designed the research and wrote the manuscript. M.F.K. conducted the experiments and analyzed the data.

ACKNOWLEDGMENTS

We thank Jaison Omoto for carefully reading the manuscript, Jacob Aptekar for experimental help and contribution to the subpanel of Figure 1M, Volker Hartenstein for confocal microscope use, Frye lab members for helpful discussion, Aljoscha Nern and Michael Reiser for lobula layer identification and kindly discussing unpublished results, and David Krantz for the VGAT antibody. This research was supported by the UCLA Edith Hyde Fellowship (M.F.K.) and NIH EY026031 (M.A.F.).

Received: October 16, 2016
Revised: December 15, 2016
Accepted: January 6, 2017
Published: February 9, 2017

REFERENCES

1. Hubel, D.H., and Wiesel, T.N. (1965). Receptive fields and functional architecture in two nonstriate visual areas (18 and 19) of the cat. J. Neurophysiol. *28*, 229–289.
2. O'Carroll, D. (1993). Feature-detecting neurons in dragonflies. Nature *362*, 541–543.
3. Nordström, K., and O'Carroll, D.C. (2006). Small object detection neurons in female hoverflies. Proc. Biol. Sci. *273*, 1211–1216.
4. Otsuna, H., and Ito, K. (2006). Systematic analysis of the visual projection neurons of Drosophila melanogaster. I. Lobula-specific pathways. J. Comp. Neurol. *497*, 928–958.
5. Aptekar, J.W., Shoemaker, P.A., and Frye, M.A. (2012). Figure tracking by flies is supported by parallel visual streams. Curr. Biol. *22*, 482–487.
6. Bahl, A., Ammer, G., Schilling, T., and Borst, A. (2013). Object tracking in motion-blind flies. Nat. Neurosci. *16*, 730–738.
7. Bahl, A., Serbe, E., Meier, M., Ammer, G., and Borst, A. (2015). Neural mechanisms for Drosophila contrast vision. Neuron *88*, 1240–1252.
8. Poggio, T., and Reichardt, W. (1976). Visual control of orientation behaviour in the fly. Part II. Towards the underlying neural interactions. Q. Rev. Biophys. *9*, 377–438.
9. Coen, P., Xie, M., Clemens, J., and Murthy, M. (2016). Sensorimotor transformations underlying variability in song intensity during Drosophila courtship. Neuron *89*, 629–644.
10. Meier, M., Serbe, E., Maisak, M.S., Haag, J., Dickson, B.J., and Borst, A. (2014). Neural circuit components of the Drosophila OFF motion vision pathway. Curr. Biol. *24*, 385–392.
11. Maisak, M.S., Haag, J., Ammer, G., Serbe, E., Meier, M., Leonhardt, A., Schilling, T., Bahl, A., Rubin, G.M., Nern, A., et al. (2013). A directional tuning map of Drosophila elementary motion detectors. Nature *500*, 212–216.
12. Ammer, G., Leonhardt, A., Bahl, A., Dickson, B.J.J., and Borst, A. (2015). Functional specialization of neural input elements to the Drosophila ON motion detector. Curr. Biol. *25*, 2247–2253.
13. Joesch, M., Schnell, B., Raghu, S.V., Reiff, D.F., and Borst, A. (2010). ON and OFF pathways in *Drosophila* motion vision. Nature *468*, 300–304.
14. Strausfeld, N.J. (1976). Atlas of an Insect Brain (Springer).
15. Panser, K., Tirian, L., Schulze, F., Villalba, S., Jefferis, G.S.X.E., Bühler, K., and Straw, A.D. (2016). Automatic segmentation of Drosophila neural compartments using GAL4 expression data reveals novel visual pathways. Curr. Biol. *26*, 1943–1954.
16. Wu, M., Nern, A., Williamson, W.R., Morimoto, M.M., Reiser, M.B., Card, G.M., and Rubin, G.M. (2016). Visual projection neurons in the Drosophila lobula link feature detection to distinct behavioral programs. eLife *5*, e21022.
17. Kim, A.J., Fitzgerald, J.K., and Maimon, G. (2015). Cellular evidence for efference copy in Drosophila visuomotor processing. Nat. Neurosci. *18*, 1247–1255.
18. Aptekar, J.W., Keleş, M.F., Lu, P.M., Zolotova, N.M., and Frye, M.A. (2015). Neurons forming optic glomeruli compute figure-ground discriminations in Drosophila. J. Neurosci. *35*, 7587–7599.
19. Mu, L., Ito, K., Bacon, J.P., and Strausfeld, N.J. (2012). Optic glomeruli and their inputs in Drosophila share an organizational ground pattern with the antennal lobes. J. Neurosci. *32*, 6061–6071.
20. Jenett, A., Rubin, G.M., Ngo, T.T.B., Shepherd, D., Murphy, C., Dionne, H., Pfeiffer, B.D., Cavallaro, A., Hall, D., Jeter, J., et al. (2012). A GAL4-driver line resource for Drosophila neurobiology. Cell Rep. *2*, 991–1001.
21. Warrant, E.J., Kelber, A., Gislén, A., Greiner, B., Ribi, W., and Wcislo, W.T. (2004). Nocturnal vision and landmark orientation in a tropical halictid bee. Curr. Biol. *14*, 1309–1318.
22. Maimon, G., Straw, A.D., and Dickinson, M.H. (2008). A simple vision-based algorithm for decision making in flying Drosophila. Curr. Biol. *18*, 464–470.
23. Agrawal, S., Safarik, S., and Dickinson, M. (2014). The relative roles of vision and chemosensation in mate recognition of Drosophila melanogaster. J. Exp. Biol. *217*, 2796–2805.
24. Zabala, F., Polidoro, P., Robie, A., Branson, K., Perona, P., and Dickinson, M.H. (2012). A simple strategy for detecting moving objects during locomotion revealed by animal-robot interactions. Curr. Biol. *22*, 1344–1350.
25. Heisenberg, M., and Wolf, R. (1984). Vision in *Drosophila*, Genetics of Microbehavior (Springer-Verlag).
26. Theobald, J.C., Ringach, D.L., and Frye, M.A. (2010). Dynamics of optomotor responses in Drosophila to perturbations in optic flow. J. Exp. Biol. *213*, 1366–1375.
27. Juusola, M., Dau, A., Song, Z., Solanki, N., Rien, D., Jaciuch, D., Dongre, S., Blanchard, F., de Polavieja, G.G., Hardie, R.C., and Takalo, J. (2016). Microsaccadic information sampling provides Drosophila hyperacute vision. bioRxiv. http://dx.doi.org/10.1101/083691.
28. Behnia, R., Clark, D.A., Carter, A.G., Clandinin, T.R., and Desplan, C. (2014). Processing properties of ON and OFF pathways for Drosophila motion detection. Nature *512*, 427–430.
29. Tuthill, J.C., Nern, A., Rubin, G.M., and Reiser, M.B. (2014). Wide-field feedback neurons dynamically tune early visual processing. Neuron *82*, 887–895.
30. Schnell, B., Joesch, M., Forstner, F., Raghu, S.V., Otsuna, H., Ito, K., Borst, A., and Reiff, D.F. (2010). Processing of horizontal optic flow in three visual interneurons of the Drosophila brain. J. Neurophysiol. *103*, 1646–1657.
31. Wiederman, S.D., Shoemaker, P.A., and O'Carroll, D.C. (2013). Correlation between OFF and ON channels underlies dark target selectivity in an insect visual system. J. Neurosci. *33*, 13225–13232.
32. Barnett, P.D., Nordström, K., and O'carroll, D.C. (2007). Retinotopic organization of small-field-target-detecting neurons in the insect visual system. Curr. Biol. *17*, 569–578.
33. Serbe, E., Meier, M., Leonhardt, A., and Borst, A. (2016). Comprehensive characterization of the major presynaptic elements to the Drosophila OFF motion detector. Neuron *89*, 829–841.
34. Strother, J.A., Nern, A., and Reiser, M.B. (2014). Direct observation of ON and OFF pathways in the Drosophila visual system. Curr. Biol. *24*, 976–983.
35. Fischbach, K.-F., and Dittrich, A.P.M. (1989). The optic lobe of Drosophila melanogaster. I. A Golgi analysis of wild-type structure. Cell Tissue Res. *258*, 441–475.
36. Buchner, E., Bader, R., Buchner, S., Cox, J., Emson, P.C., Flory, E., Heizmann, C.W., Hemm, S., Hofbauer, A., and Oertel, W.H. (1988). Cell-specific immuno-probes for the brain of normal and mutant Drosophila melanogaster. I. Wildtype visual system. Cell Tissue Res. *253*, 357–370.
37. Harrison, J.B., Chen, H.H., Sattelle, E., Barker, P.J., Huskisson, N.S., Rauh, J.J., Bai, D., and Sattelle, D.B. (1996). Immunocytochemical

mapping of a C-terminus anti-peptide antibody to the GABA receptor subunit, RDL in the nervous system in Drosophila melanogaster. Cell Tissue Res. *284*, 269–278.

38. Mauss, A.S., Meier, M., Serbe, E., and Borst, A. (2014). Optogenetic and pharmacologic dissection of feedforward inhibition in Drosophila motion vision. J. Neurosci. *34*, 2254–2263.

39. Warzecha, A.K., Egelhaaf, M., and Borst, A. (1993). Neural circuit tuning fly visual interneurons to motion of small objects. I. Dissection of the circuit by pharmacological and photoinactivation techniques. J. Neurophysiol. *69*, 329–339.

40. Wiederman, S.D., Shoemaker, P.A., and O'Carroll, D.C. (2008). A model for the detection of moving targets in visual clutter inspired by insect physiology. PLoS ONE *3*, e2784.